

# A Recombinant Chimeric Epidermal Growth Factor-like Module with High Binding Affinity for Integrins\*

Received for publication, February 11, 2003, and in revised form, March 21, 2003  
Published, JBC Papers in Press, March 24, 2003, DOI 10.1074/jbc.M301470200

Fanny Vella‡, Nicole M. Thielens‡, Beate Bersch§, Gérard J. Arlaud‡, and Philippe Frachet‡¶

From the ‡Laboratoire d'Enzymologie Moléculaire and §Laboratoire de Résonance Magnétique Nucléaire, Institut de Biologie Structurale Jean-Pierre Ebel, (Commissariat à l'Energie Atomique CNRS, Université Joseph Fourier), Grenoble 38027 Cedex 1, France

**Integrins are cell surface receptors involved in numerous pathological processes such as metastasis invasion and abnormal angiogenesis. To target these receptors, the epidermal growth factor (EGF)-like domain of human complement protease C1r was used as a natural scaffold to design chimeric modules containing the RGD motif. Here we report a high yield bacterial expression system and its application to the production of two such modules, EGF-RGD and V2, the latter variant mimicking the RGD-containing domain of disintegrins. These modules were characterized chemically, and their biological activity was investigated by cellular assays using various Chinese hamster ovary cell lines expressing  $\beta_1$  and  $\beta_3$  integrins and by surface plasmon resonance spectroscopy. Remarkably, the modifications leading to the V2 variant had differential effects on the interaction with  $\beta_3$  and  $\beta_1$  integrins. The disintegrin-like V2 module exhibited enhanced binding affinities compared with EGF-RGD, with  $K_D$  values of 7.2 nM for  $\alpha_5\beta_1$  (a 4-fold decrease) and 3.5 nM for  $\alpha_v\beta_3$  (a 1.5-fold decrease), comparable with the values determined for natural integrin ligands. Analysis by NMR spectroscopy also revealed a differential dynamic behavior of the RGD motif in the EGF-RGD and V2 variants, providing insights into the structural basis of their relative binding efficiency. These novel RGD-containing EGF modules open the way to the design of improved variants with selective affinity for particular integrins and their use as carriers for other biologically active modules.**

Targeting the appropriate cell type is a major challenge in cancer and cell therapy. Integrins, a family of cell receptors for plasma proteins, extracellular matrix proteins, and cell surface ligands (1–3), are potential targets for this purpose, because they are expressed by all cell types and are involved in many physiological functions including cell adhesion, proliferation, or differentiation, and pathological processes such as metastasis invasion, abnormal angiogenesis and vascularization, or thrombosis (4). In mammals, 18  $\alpha$  and eight  $\beta$  subunits assemble into 24 different non-covalent  $\alpha\beta$  heterodimers that mediate bidirectional signals through the cell membrane. In response to cell activation, “inside-out” signals control the level of binding affinity for the ligand. In turn, ligand binding induces

rearrangements in integrin structure that trigger “outside-in” signaling pathways (5). Extensive cross-talk also takes place between integrin and growth factor receptor signaling pathways (6, 7), influencing most integrin functions.

The  $\beta_1$  integrin subset, comprising the major fibronectin receptor  $\alpha_5\beta_1$ , is the most widely expressed. The  $\beta_3$  subset includes the fibrinogen receptor  $\alpha_{IIb}\beta_3$ , present on platelets and megakaryocytes, and  $\alpha_v\beta_3$ , originally described as the vitronectin receptor, which also binds a variety of matrix proteins including fibronectin and fibrinogen. Integrin  $\alpha_v\beta_3$  is expressed on vascular cells during angiogenesis (8, 9) and is also present in the adult on activated leukocytes, osteoclasts, and macrophages, where it participates in bone resorption and ingestion of apoptotic cells. The expression of various integrins has been shown to be deregulated in a number of cancer cells and invasive tumors and is thought to participate in the malignancy phenotypes (10–14). Thus, a decreased expression of  $\alpha_5\beta_1$  appears to increase the degree of tumorigenicity. In contrast, the level of  $\alpha_v\beta_3$  is correlated with the survival and metastatic activity of tumor cells (10, 15) and has an important role in angiogenesis in tumors (11). Integrins, particularly  $\alpha_v\beta_3$ , are therefore considered as appropriate targets for cancer therapy. Intracellular drug or DNA delivery by integrin-targeted vectors has been shown to use the endocytic pathway (16).

Many integrins, particularly  $\alpha_5\beta_1$  and  $\alpha_v\beta_3$ , recognize the RGD motif as the critical determinant in their ligands (17). The structural basis of this interaction has been documented recently (18, 19) from the crystal structure of the extracellular domain of  $\alpha_v\beta_3$  alone or in complex with an RGD ligand. Among the natural ligands of integrins, disintegrins (20, 21), which are snake venom polypeptides related to the multifunctional ADAMs protein family (22), are potent inhibitors of integrin function. They block platelet aggregation through interaction with  $\alpha_{IIb}\beta_3$  and also inhibit  $\alpha_v\beta_3$  and  $\alpha_5\beta_1$  functions. Disintegrins are cysteine-rich peptides of 48–84 amino acid residues, and their activities are directly related to the presence of an RGD or a related sequence in a large flexible loop (23, 24) and mimic natural integrin ligands such as fibronectin, fibrinogen, or vitronectin. Integrin-targeted molecules developed in the recent years include antibodies, cyclic peptides, peptidomimetics, viruses, and small molecules (25). With the aim to develop a molecule able to interact with high affinity with integrins, we chose to introduce the critical RGD sequence in a stable, structurally compatible small protein scaffold. The EGF<sup>1</sup>-like mod-

\* The costs of publication of this article were defrayed in part by the payment of page charges. This article must therefore be hereby marked “advertisement” in accordance with 18 U.S.C. Section 1734 solely to indicate this fact.

¶ To whom correspondence should be addressed: Laboratoire d'Enzymologie Moléculaire, Institut de Biologie Structurale Jean-Pierre Ebel, 41 rue Jules Horowitz, Grenoble 38027 Cedex 1, France. Tel.: 33-4-38-78-95-79; Fax: 33-4-38-78-54-94; E-mail: philippe.frachet@ibs.fr.

<sup>1</sup> The abbreviations used are: EGF, epidermal growth factor; CHO, Chinese hamster ovary; HPLC, high pressure liquid chromatography; PBS, phosphate-buffered saline; NOE, nuclear Overhauser effect; Trx, thioredoxin; HSQC, <sup>1</sup>H-detected heteronuclear single-quantum coherence; NOESY, NOE spectroscopy; TOCSY, total correlation spectroscopy; D-RGDW, the RGDW peptide with the D-isomer of arginine.

ule of human complement protease C1r appeared as a good candidate for this purpose, because it is stabilized by three disulfide bridges and features a large, structurally independent, and mobile loop between its first two cysteine residues (26, 27). A further advantage of EGF-like modules is their natural ability to associate with a variety of other module types, as seen in many natural proteins (28, 29), which opens the possibility of designing multimodular chimeric proteins.

In a previous study (30), we showed, using chemical synthesis, that insertion of the GRGDSP motif of fibronectin into the human C1r EGF module resulted in a chimeric molecule with the ability to mediate attachment of CHO cells expressing the  $\beta_1$  class of integrins. In the present study we describe an efficient bacterial expression system that allows high yield production of chimeric EGF-like modules. This strategy was applied to the production of two modules, including a new variant designed to mimic the RGD-containing domain of disintegrins. Functional characterization of the recombinant modules by various methods including cell adhesion and surface plasmon resonance analysis indicates preferential binding to  $\beta_3$  integrins, whereas NMR spectroscopy provides insights into the structural basis of their relative binding efficiency.

#### EXPERIMENTAL PROCEDURES

##### Cell Lines, Antibodies, Peptides, and Reagents

The cell lines CHO (ATCC number CCL-61),  $\beta_3$ -CHO, and  $\alpha_{\text{IIb}}\beta_3$ -CHO (stably established by transfection with human megakaryocyte  $\beta_3$  and/or  $\alpha_{\text{IIb}}$  cDNA (31)) were cultured in Glutamax Dulbecco's modified Eagle's medium (Invitrogen) containing 7.5% (v/v) fetal calf serum, 1% penicillin, and 1% streptomycin. The medium was supplemented with 800  $\mu\text{g/ml}$  of G418 (Invitrogen) when necessary. Peptides D-RGDW and RGEs were supplied by M.-H. Charon (Commissariat à l'Énergie Atomique, Grenoble, France). Polyclonal anti- $\alpha_v$  antibodies (AB1930) were from Chemicon International (Temecula, CA). Polyclonal anti-C1r antibodies recognizing native human C1r were raised in rabbits (32). Integrins  $\alpha_v\beta_3$  from human placenta and  $\alpha_5\beta_1$  from human smooth muscle and placenta tissue were purchased from Chemicon in the octyl- $\beta$ -D-glucopyranoside formulation. The purity and integrity of each integrin sample were checked by SDS-PAGE analysis.

##### Preparation of the Trx Fusion Proteins

**Cloning**—The cDNA sequence coding for the human C1r EGF module was amplified by PCR using the complete C1r cDNA (33) as a template. A *Nde*I site and codons for the amino acid sequence IEGR (factor Xa cleavage site) were introduced at the 5' end. The 3' end consisted of a stop codon and an *Eco*RI site. The PCR product was then ligated to the *Nde*I and *Eco*RI sites of the pET 28b vector (Novagen, Madison, WI). The codons for the GRGDSP amino acid sequence were then introduced by the PCR overlap extension method (34, 35) to produce the EGF-RGD and V2 modules (see Fig. 1). A *Sac*II restriction site was introduced into the PCR primers to allow mutation screening. The *Nco*I/*Xho*I fragments isolated from the pET28b recombinant plasmids were then introduced into the same sites of the linearized pET32a vector (Novagen). The resulting vectors, pET32-C1r EGF, pET32-EGF-RGD, and pET32-V2 predicted a protein containing the 109 amino acids of thioredoxin A, a thrombin cleavage site, a first histidine tag, an enterokinase cleavage site, a second histidine tag, and a factor Xa cleavage site, followed by the EGF module sequence (C1r EGF, EGF-RGD, or V2). The constructs were checked by double-stranded DNA sequencing (Genome Express, Meylan, France).

**Protein Expression and Isolation**—Recombinant pET32 vectors were introduced by transformation into *Escherichia coli* BL21trxB(DE3) (Novagen), and bacteria were cultured at 37 °C in a Luria-Bertani medium to an  $A_{595}$  of 0.4. Protein production was induced with 1 mM isopropyl-1-thio- $\beta$ -D-galactopyranoside for 5 h at 37 °C. Bacteria were collected by centrifugation, suspended in 1/25 culture volume of 20 mM  $\text{Na}_2\text{HPO}_4$ , 0.5 M NaCl, 50 mM imidazole, pH 7.4, containing an anti-protease mixture (Roche Molecular Biochemicals), sonicated, and then centrifuged at 40,000  $\times g$  for 30 min at 4 °C. The clarified fraction was added to a histidine-binding nickel-Sepharose Fast Flow resin (Amersham Biosciences) packed in an Econo-Pack column (Bio-Rad). After extensive washing with 50 mM imidazole, 20 mM  $\text{Na}_2\text{HPO}_4$ , pH 7.4, elution was achieved by 100–500 mM imidazole solutions in the same buffer.

The eluted samples were pooled and dialyzed against 0.05% (v/v) trifluoroacetic acid and freeze-dried. For production of recombinant modules isotopically labeled with  $^{15}\text{N}$ , freshly transformed bacteria were grown in an M9 minimal medium complemented with 1 g/liter  $^{15}\text{NH}_4\text{Cl}$ , 4 g/liter glucose and supplemented with 0.1 mM  $\text{MnCl}_2$ , 0.05 mM  $\text{ZnCl}_2$ , 0.05 mM  $\text{FeCl}_3$ , and a vitamin solution according to Jansson *et al.* (36).

##### Factor Xa Cleavage, Protein Purification, and Analytical Methods

The recombinant EGF modules were released from thioredoxin by digestion of the fusion proteins (10  $\mu\text{M}$  in 50 mM Tris-HCl, 100 mM NaCl, 5 mM  $\text{CaCl}_2$ , pH 8.0) with factor Xa (1 units/50  $\mu\text{g}$ ) for 16 h at 25 °C. The cleavage mixture was then analyzed and purified by reverse-phase HPLC using an analytical (0.46  $\times$  25 cm) or a semi-preparative (2.2  $\times$  25 cm) Vydac C18 column as described previously (30). Fractions were analyzed by electrospray mass spectrometry, and the purified material was controlled by N-terminal sequence analysis (30). The chimeric EGF modules were freeze-dried and stored at 4 °C until use. Protein concentrations were determined by absorbance measurement at 280 nm using molar extinction coefficients of 18,260  $\text{M}^{-1}\text{cm}^{-1}$  for Trx module fusions and of 4,200  $\text{M}^{-1}\text{cm}^{-1}$  for the cleaved modules.

##### Adhesion Assays

Adhesion assays were performed in plastic microtitration plates (Nunc, Inc.). Wells were coated overnight at 4 °C with the recombinant protein modules (1–100  $\mu\text{g/ml}$  in PBS) or fibronectin (BD Biosciences) (25  $\mu\text{g/ml}$  in PBS), and free binding sites were blocked with 3% bovine serum albumin. Cells were harvested at 60–80% of confluence using trypsin-EDTA (Invitrogen) and then allowed to attach for 1 h at 37 °C using  $5 \times 10^5$  cells in 100  $\mu\text{l}$  of medium/well. Non-adherent cells were removed by three washes in PBS, and the amount of attached cells was determined using a cell quantification kit by adding 20  $\mu\text{l}$  of MTS reagent (Promega) to each well. After color development, plates were read on a Dynatech reader at 490 nm. Assays were run in triplicate, and nonspecific attachment to BSA alone (less than 5% of total adhesion) was subtracted from all measurements. Control experiments done with the Trx-C1r EGF or C1r EGF constructs showed no significant adhesion. For inhibition experiments, competitors at various concentrations were preincubated with the cells for 15 min at 4 °C before attachment. For inhibition by the soluble V2 module, fibrinogen (Stago, Asnières, France) and fibronectin were used at concentrations yielding half-maximal adhesion, namely 5 and 16  $\mu\text{g/ml}$ , respectively.

##### Staining of Actin Fibers

Glass slides were coated overnight at 4 °C with fibronectin (25  $\mu\text{g/ml}$ ) or the EGF-RGD and V2 modules (100  $\mu\text{g/ml}$ ) and then coated with 3% bovine serum albumin for 2 h at 37 °C. Harvested cells were suspended in Dulbecco's modified Eagle's medium with serum and then plated onto the coated slides for 2 h at 37 °C. After the incubation period, cells were fixed for 10 min in PBS containing 3% paraformaldehyde and 2% saccharose and then permeabilized for 20 min in PBS containing 1% Triton X-100 (w/v). After three washes in PBS, actin staining was performed using rhodamine-labeled phalloidin (Sigma). All incubations were performed at room temperature. Stained cells were observed under a laser confocal fluorescence microscope (Leica). Polylysine (70  $\mu\text{g/ml}$ ) was used as a negative control for stress fiber formation.

##### Surface Plasmon Resonance Spectroscopy and Data Evaluation

Surface plasmon resonance measurements were performed using a BIAcore 3000 instrument (BIAcore AB, Uppsala, Sweden). The running buffer for protein immobilization was 145 mM NaCl, 5 mM EDTA, 10 mM HEPES, pH 7.4. The recombinant EGF-RGD and V2 modules were diluted to 200–400  $\mu\text{g/ml}$  in 10 mM sodium acetate, pH 4.0, and immobilized onto the carboxymethylated dextran surface of a CM5 sensor chip (BIAcore AB) using the amine coupling chemistry (BIAcore AB amine coupling kit). Binding of the purified  $\alpha_v\beta_3$  and  $\alpha_5\beta_1$  integrins was measured over 2,500 resonance units of immobilized EGF-RGD and 1,400 resonance units of immobilized V2 at a flow rate of 20  $\mu\text{l/min}$  in the running buffer (150 mM NaCl, 25 mM Tris-HCl, pH 7.4, 0.1 mM  $\text{CaCl}_2$ , 1 mM  $\text{MgCl}_2$ , 10 mM octyl- $\beta$ -D-glucopyranoside). This buffer was identical to that of the purchased integrins, including divalent cations and detergent, to avoid sample modification. Regeneration of the surfaces was achieved by injection of 10  $\mu\text{l}$  of a 10 mM solution of the D-RGDW peptide. The specific binding signal shown was obtained by subtracting the background signal, routinely obtained by injection of the protein sample over an activated-deactivated surface. Immobilized bovine serum albumin or the unmodified C1r EGF module (30) showed no integrin binding. The data were analyzed by global fitting to a 1:1

Langmuir binding model of both the association and dissociation phases for several concentrations simultaneously, using the BIAevaluation 3.2 software (BIAcore AB). The apparent equilibrium dissociation constants ( $K_D$ ) were calculated from the ratio of the dissociation and association rate constants ( $k_{off}/k_{on}$ ). The data presented for both  $\alpha_v\beta_3$  and  $\alpha_5\beta_1$  correspond to a representative series of binding studies performed on the same sensor chip. In each case, similar results were reproduced from at least three independent experiments, using different integrin batches and different sensor chips.

#### Polyacrylamide Gel Electrophoresis and Immunoblotting

SDS-PAGE analysis was performed as described by Laemmli (37). Western blot analysis and immunochemical detection of the recombinant proteins were carried out as described by Rossi *et al.* (38). Chemiluminescence revelation was performed using the ECL kit (Amersham Biosciences) and an anti-rabbit IgG coupled to horseradish peroxidase.

#### NMR Spectroscopy

The EGF-RGD and V2 modules were dissolved at a final concentration of  $\sim 1$  mM in 50 mM sodium phosphate, pH 6.7, containing 10% D<sub>2</sub>O. All NMR experiments were acquired on Varian INOVA 400 and 800 spectrometers. For the assignment of the amide proton and nitrogen chemical shifts, <sup>15</sup>N-edited HSQC and three-dimensional NOESY-HSQC experiments, as well as two-dimensional, <sup>15</sup>N-decoupled TOCSY and NOESY experiments were acquired at 800 MHz. TOCSY and NOESY mixing times were 70 and 150 ms, respectively. All chemical shifts were referenced with respect to 2,2-dimethyl-2-silapentane-5-sulfonate sodium salt using the <sup>1</sup>H/<sup>15</sup>N frequency ratio of the zero point of 0.101329118 according to Markley *et al.* (39). Relaxation measurements were performed at 400 Mhz. The <sup>15</sup>N heteronuclear  $R_1$  and  $R_{1\rho}$  relaxation rates and the <sup>1</sup>H-<sup>15</sup>N NOE were measured using standard pulse sequences (40). Two-dimensional <sup>1</sup>H-<sup>15</sup>N correlation spectra were acquired with 1024 (<sup>1</sup>H) and 100 (<sup>15</sup>N) complex points and 16 ( $R_1$  and  $R_{1\rho}$ ) or 64 scans (<sup>1</sup>H-<sup>15</sup>N NOE) per  $t_1$  increment. The relaxation-caused magnetization delay was sampled at nine different time points for  $R_1$  (0.014, 0.072, 0.131, 0.189, 0.248, 0.306, 0.393, 0.466, and 0.598 s) and seven time points for  $R_{1\rho}$  (0.008, 0.04, 0.072, 0.104, 0.136, 0.168, and 0.2 s). The first time point was repeated at the end to check for sample and measurement stability and to evaluate experimental errors. For the steady-state <sup>1</sup>H-<sup>15</sup>N NOE measurements, two spectra were acquired with and without proton saturation in an interleaved manner. The recycle delays were set to 1 s ( $R_1$  and  $R_{1\rho}$ ) and 5 s (<sup>1</sup>H-<sup>15</sup>N NOE). Data processing and peak picking were performed using the FELIX 2000 software (Accelrys Inc.). The <sup>15</sup>N  $R_1$  and  $R_{1\rho}$  relaxation rates were determined from peak intensities rather than from peak volumes, using a non-linear least-squares fit to a two-parameter single exponential function  $I(t) = I(0)\exp(Rt)$ , where  $I(t)$  is the peak intensity after a relaxation delay of time  $t$ , and  $I(0)$  is the initial peak intensity. Uncertainties in the resulting  $R_1$  and  $R_{1\rho}$  values were estimated by Monte-Carlo simulations with 1000 random Gaussian noise iterations, taking into account the experimental noise from the spectra. The transverse relaxation rate constants  $R_2$  were calculated from  $R_{1\rho}$  rate constants using the relation,  $R_{1\rho} = \cos^2(\theta)R_2 + \sin^2(\theta)R_1$ , where  $\theta = \tan^{-1}(2\pi\Delta\nu/\gamma_N B_1)$ , and  $\Delta\nu$  is the frequency difference between the <sup>15</sup>N carrier and the frequency of the observed nitrogen. The steady-state heteronuclear NOE were determined from the ratio of the peak intensities measured in experiments acquired with and without proton saturation.

#### Interaction between Integrins and Nickel-Sepharose-Trx Modules

Cells were lysed on the culture plate for 1 h at 4 °C in PBS containing 1 mM CaCl<sub>2</sub>, 1 mM MgCl<sub>2</sub>, 1% Triton X-100, and an anti-protease mixture (Roche Molecular Biochemicals). The cell extract was clarified by centrifugation at 13,000  $\times g$  for 15 min at 4 °C. Proteins were quantified using a micro BCA assay (Pierce). Fractions of the cell extract, containing 1 mg of total proteins, were incubated for 2.5 h at room temperature with an equal volume of a nickel-Sepharose-Trx module resin prepared by mixing 1 mg of Trx module fusion protein with 400  $\mu$ l of chelating Sepharose. After extensive washes using PBS containing 1 mM CaCl<sub>2</sub>, 1 mM MgCl<sub>2</sub>, and 0.05% (w/v) Tween 20, bound proteins were recovered by elution with 1 ml of PBS containing 10 mM EDTA and 50 mM NaCl. Following trichloroacetic acid precipitation, samples were analyzed by SDS-PAGE under non-reducing conditions and Western blotting using anti- $\alpha_v$  antibodies and chemiluminescence detection.

## RESULTS

### Engineering, Production, and Biochemical Characterization of Recombinant EGF-RGD Modules—Our previous data based

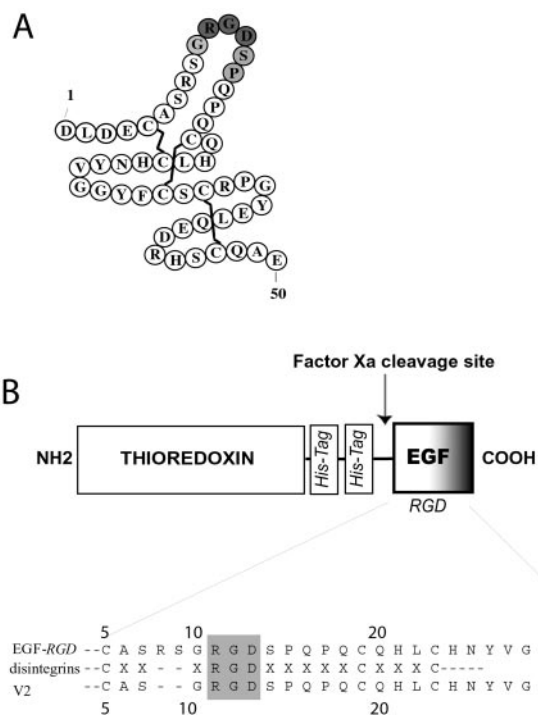


**FIG. 1. Design of the chimeric EGF-RGD modules.** *A*, schematic representation of the chimeric EGF-RGD module highlighting the inserted GRGDSP motif and the Cys<sup>1</sup>-Cys<sup>3</sup>, Cys<sup>2</sup>-Cys<sup>4</sup>, Cys<sup>5</sup>-Cys<sup>6</sup> disulfide bridge pattern characteristic of EGF-like modules. *B*, schematic diagram of the Trx-EGF-RGD constructs and homology between the V2 variant and the RGD-containing loop of disintegrins. Note that, for the sake of clarity (especially for NMR experiments; see Fig. 8), the numbering is identical for both modules, except for residues 8 and 9, which are not present in the V2 sequence.

on a synthetic EGF-RGD module (30) led us to develop a recombinant strategy to overproduce the original module and a variant designed to mimic the structure of disintegrins (Fig. 1A). Based on the alignment of the RGD-containing loop of the EGF-RGD module with the consensus sequence of the corresponding region of disintegrins (Fig. 1B), a variant termed V2 was designed by shortening the loop to the same length as in disintegrins. To produce soluble and well folded recombinant proteins we chose the pET 32/*E. coli* BL21 Trx B (DE3) system, which uses thioredoxin (TrxA) as a gene fusion partner. As shown in Fig. 1B, a factor Xa cleavage site was introduced between the fusion protein and the EGF module. As illustrated in the case of Trx-EGF-RGD, both fusion proteins were overproduced after induction with isopropyl-1-thio- $\beta$ -D-galactopyranoside (Fig. 2A). Purification was carried out from clarified lysates obtained after sonication of the cell pellets. The Trx-EGF-RGD and Trx-V2 fusion proteins bound to nickel-Sepharose columns and were subsequently eluted using 200–300 mM imidazole (Fig. 2B). Western blotting realized on the different fractions using polyclonal anti-C1r antibodies revealed a major band of around 30 kDa in both cases (Fig. 2C), consistent with the calculated values (25,508.2 Da for Trx-EGF-RGD and 25,264.9 Da for Trx-V2). Two bands of about 66 and 94 kDa were observed in each case, likely corresponding to dimeric and trimeric forms of the recombinant proteins.

Cleavage with factor Xa efficiently released the recombinant EGF modules from thioredoxin. The isolated modules were then purified to homogeneity by reverse-phase HPLC (Fig. 2D), and their disulfide bridges were checked by peptide mapping as described previously (30), establishing a Cys<sup>1</sup>-Cys<sup>3</sup>, Cys<sup>2</sup>-Cys<sup>4</sup>, Cys<sup>5</sup>-Cys<sup>6</sup> pattern characteristic of EGF-like modules (28). Analysis by electrospray mass spectrometry confirmed the

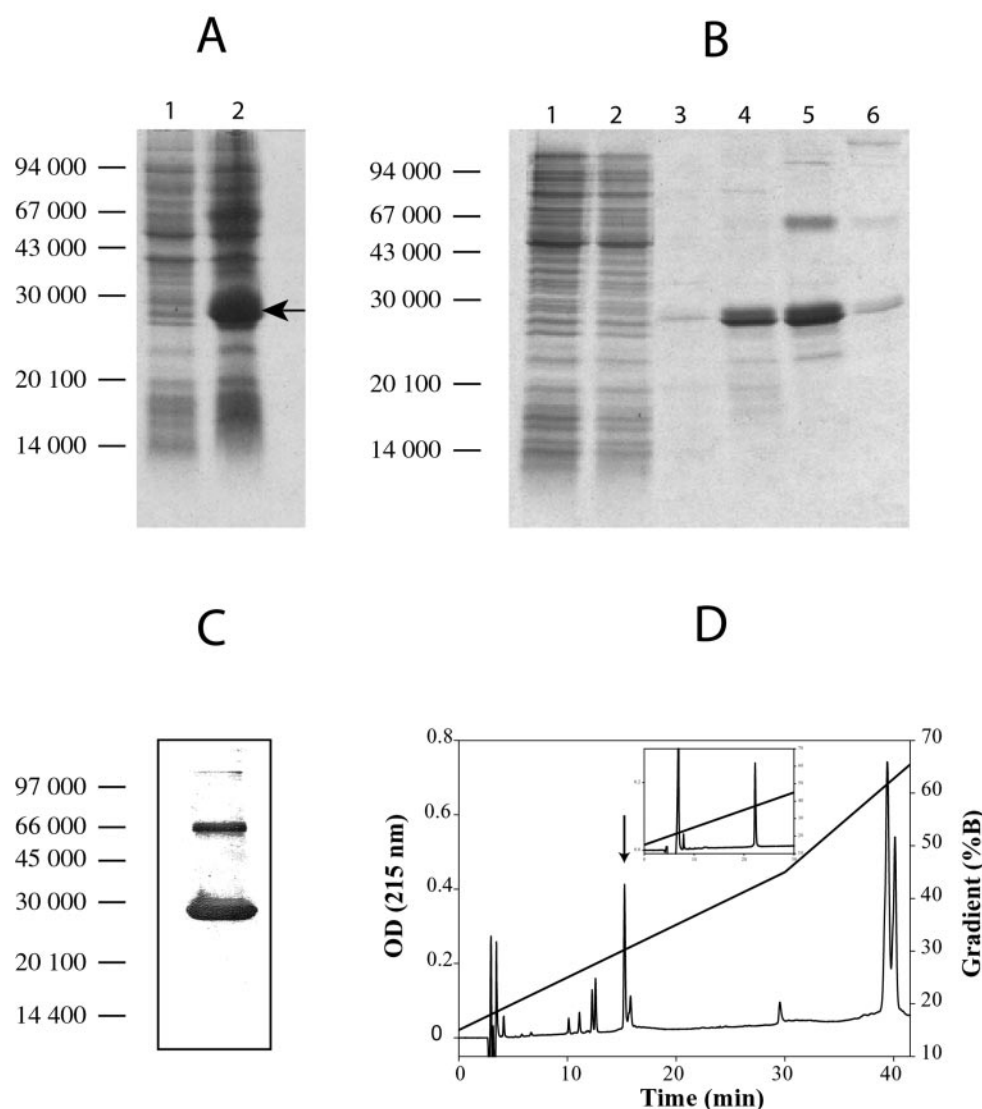
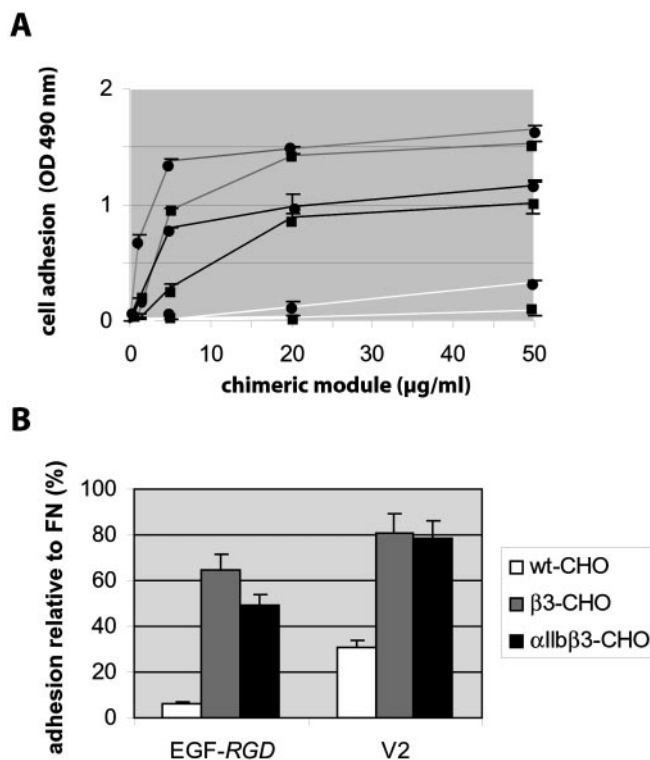


FIG. 2. **Expression and purification of the recombinant modules.** A, SDS-PAGE analysis of the fusion protein Trx-EGF-RGD expressed in *E. coli* BL21 Trx B (DE3). Positions of molecular mass markers (expressed in Da) are shown. Analyses of total bacterial extracts before induction (lane 1) and after induction with 1 mM isopropyl-1-thio- $\beta$ -D-galactopyranoside for 5 h (lane 2). B, induced cultures were submitted to sonication, and the soluble recombinant protein was purified onto a nickel-Sepharose column and analyzed by SDS-PAGE. Positions of molecular mass markers are shown. Lane 1, unbound proteins. Lanes 2–6, material eluted with 50, 100, 200, 300, and 500 mM imidazole. All samples in A and B were analyzed under non-reducing conditions on 12.5% polyacrylamide gels and stained with Coomassie Blue. C, pooled 200 and 300 mM imidazole fractions were analyzed by Western blot using polyclonal anti-C1r antibodies, and detection was performed with anti-rabbit IgG coupled to horseradish peroxidase. Positions of molecular mass markers are indicated. D, reverse-phase HPLC analysis of the reaction mixture after factor Xa cleavage. The arrow shows the position of the expected EGF-RGD peptide. The inset shows analysis of the purified peptide. Analyses were performed on a Vydac C18 column, at a flow rate of 1 ml/min, using increasing gradients of Solvent B (0.09% acetonitrile in 0.1% trifluoroacetic acid) in Solvent A (0.1% trifluoroacetic acid). The analyses shown are for the EGF-RGD module. Similar results were obtained for the V2 variant and the unmodified C1r EGF module.

identity and homogeneity of the recombinant EGF-RGD and V2 modules, yielding reconstructed molecular masses of  $5,627.35 \pm 0.53$  and  $5,384.59 \pm 0.53$  Da, respectively, consistent with the calculated values (5,628.0 and 5,384.8 Da, respectively). The yields obtained were routinely 50–70 mg per liter of culture for the Trx fusion proteins, resulting in 2–4 mg of the HPLC-purified isolated modules.

**EGF-RGD Modules Promote Cell Adhesion of CHO Cell Lines Expressing  $\beta_1$  and  $\beta_3$  Integrins**—To evaluate the ability of the chimeric EGF modules to promote integrin-mediated cell adhesion, we used a panel of related CHO cell lines expressing different integrins. Wild-type CHO cells express  $\alpha_5\beta_1$  as a major integrin and do not express  $\beta_3$  or  $\beta_2$  integrins;  $\beta_3$ -CHO cells produce a hybrid (hamster/human)  $\alpha_V/\beta_3$  heterodimer;  $\alpha_{IIB}\beta_3$ -CHO (31, 41, 42) express endogenous  $\alpha_5\beta_1$ , weakly the hybrid (hamster/human)  $\alpha_V/\beta_3$ , and predominantly the human

$\alpha_{IIB}\beta_3$  integrins. Preliminary experiments indicated that the Trx fusion proteins and the isolated chimeric EGF modules supported cell adhesion in a similar manner, indicating that thioredoxin did not alter the adhesion properties of the EGF modules. Adhesion assays were performed on plates coated with the isolated modules and indicated that both  $\beta_3$ -transfected cell lines had the ability to bind to the chimeric modules, whether in the presence or absence of serum. In contrast, whereas wild-type CHO cells bound to fibronectin in the absence of serum, their adhesion to the EGF-RGD and V2 modules was strictly dependent on the presence of serum. Subsequent comparative adhesion assays were therefore performed using a serum-supplemented medium. As shown in Fig. 3A, wild-type CHO cells and the  $\beta_3$ -transfected CHO cell lines bound specifically to the coated chimeric modules in a dose-dependent manner. The EGF-RGD module induced only weak



**FIG. 3. Comparative adhesion of different cell lines to the EGF-RGD and V2 modules.** Wild-type (*wt*) CHO cells,  $\beta_3$ -CHO cells, and  $\alpha_{IIb}\beta_3$ -CHO cells were allowed to attach to fibronectin, the EGF-RGD, and V2 modules for 1 h at 37 °C. The amount of adherent cells was determined as described under "Experimental Procedures." Non-specific adhesion on bovine serum albumin was subtracted. *A*, adhesion of wild-type CHO (*white lines*),  $\beta_3$ -CHO (*gray lines*), and  $\alpha_{IIb}\beta_3$ -CHO cells (*black lines*) were measured on EGF-RGD (■) or V2 (●) immobilized at different concentrations. The data shown represent the mean value  $\pm$  S.D. of triplicate experiments. *B*, adhesion was performed at a saturating concentration of the chimeric modules (100  $\mu$ g/ml) and compared with fibronectin. Results are expressed relative to the adhesion achieved on fibronectin for each cell line. The data shown represent the mean value  $\pm$  S.D. of three independent experiments.

binding of wild-type CHO cells, whereas adhesion of  $\beta_3$ -CHO and  $\alpha_{IIb}\beta_3$ -CHO cells reached much higher levels. The V2 variant yielded a similar pattern but with higher adhesion values for the three cell lines. Further experiments were conducted at a saturating concentration (100  $\mu$ g/ml) of modules, and binding was compared with fibronectin (Fig. 3*B*). Similar results were obtained under these conditions, with adhesion values on V2 reaching about 80% relative to fibronectin in the case of  $\beta_3$ -CHO and  $\alpha_{IIb}\beta_3$ -CHO cells. Cell adhesion was totally inhibited by a 20  $\mu$ M concentration of a RGDW peptide and insensitive to a RGEW peptide. In addition, the unmodified C1r EGF module showed no significant cell binding activity, indicating that the observed cell adhesion was strictly RGD-dependent. It was concluded from these data that (i) V2 is a better ligand than EGF-RGD, especially in the case of wild-type CHO cells, which only express  $\beta_1$  integrins; (ii) adhesion involves both  $\beta_1$  and  $\beta_3$  integrins, the latter being clearly responsible for the enhanced adhesion achieved with  $\beta_3$ -CHO and  $\alpha_{IIb}\beta_3$ -CHO cells; (iii) as  $\alpha_{IIb}\beta_3$ -CHO cells predominantly express  $\alpha_{IIb}\beta_3$  and only weakly  $\alpha_v\beta_3$ , adhesion by these cells likely involves mainly the former of these integrins. Further support for this hypothesis came from the inhibitory effect of peptide D-RGDW, known to block  $\alpha_{IIb}\beta_3$  preferentially to  $\alpha_v\beta_3$  (43), which was three-four times more efficient in inhibiting adhesion of  $\alpha_{IIb}\beta_3$ -CHO cells than of  $\beta_3$ -CHO cells to the EGF-RGD and V2 modules (Table I).

**Stress Fiber Formation on CHO Cell Lines Plated on Recombinant EGF-RGD Modules**—We next tested the ability of the

**TABLE I**  
Inhibition by D-RGDW of cell adhesion to the EGF-RGD and V2 modules

Cells were preincubated for 15 min at 4 °C with D-RGDW peptide at various concentration and then allowed to attach for 1 h at 37 °C onto microwells coated with Trx-EGF-RGD or Trx-V2. Adhesion was measured as described under "Experimental Procedures." IC<sub>50</sub> was determined as the concentration of D-RGDW yielding 50% of the maximum inhibition.

|                            | IC <sub>50</sub><br>Trx-EGF-RGD | Trx-V2 |
|----------------------------|---------------------------------|--------|
|                            | $\mu$ g/ml                      |        |
| $\alpha_{IIb}\beta_3$ -CHO | 5.2                             | 6.7    |
| $\beta_3$ -CHO             | 13.8                            | 25     |

EGF-RGD and V2 modules to induce cellular signaling, as assessed by the visualization of actin stress fibers by immunostaining and confocal microscopy. Wild-type and  $\beta_3$ -transfected CHO cells plated on fibronectin all showed characteristic cell spreading and organization of actin stress fibers (Fig. 4, *A*, *D*, and *G*). When bound to the chimeric modules, wild-type CHO cells adopted a less spreading morphology, and their actin filaments did not form organized stress fibers (Fig. 4, *B* and *C*). In contrast,  $\alpha_{IIb}\beta_3$ -CHO cells and  $\beta_3$ -CHO cells attached to EGF-RGD or V2 both displayed a typical spreading morphology along with a characteristic network of parallel actin fibers (Fig. 4, *E*, *F*, *H*, and *I*), similar to the morphology observed on fibronectin. These results provided evidence for the ability of the chimeric modules to support both cell adhesion and spreading. Based on the differential behavior of  $\beta_3$ -transfected cells compared with wild-type cells, it was likely that cellular signaling involved  $\beta_3$  integrins as major receptors.

**Inhibitory Effect of the V2 Module on Cell Adhesion**—To further investigate its functional properties, the chimeric V2 module was used as a soluble competitor for cell adhesion to natural ligands. As described under "Experimental Procedures," these experiments were performed in serum-free medium to avoid inhibition by serum matrix proteins. The different CHO cell lines used in this study express  $\alpha_5\beta_1$ , the major receptor for fibronectin, which also binds to fibrinogen,  $\alpha_v\beta_1$ , specific to fibronectin,  $\alpha_v\beta_3$ , which recognizes a variety of ligands including fibronectin and fibrinogen, and  $\alpha_{IIb}\beta_3$ , which in its resting state binds to surface-coated fibrinogen. Parallel inhibition assays were conducted using fibronectin and fibrinogen as ligands. Control experiments showed that the unmodified C1r EGF module had no effect on cell adhesion to fibronectin and fibrinogen (Fig. 5). When cells were plated on fibronectin, inhibition by V2 reached a maximal level of about 20% (Fig. 5*A*). On fibrinogen (Fig. 5*B*) V2 had a dose-dependent and more pronounced inhibitory effect, reaching at 2  $\mu$ M concentration maximum inhibition levels of 60% for  $\beta_3$ -CHO and wild-type CHO cells and of 40% for  $\alpha_{IIb}\beta_3$ -CHO cells. These results demonstrated the ability of the recombinant V2 module to prevent interaction of integrins with their natural ligands. The weak inhibition observed on fibronectin and the strong inhibition observed on fibrinogen provided further support for a major involvement of  $\beta_3$  integrins, compared with  $\beta_1$  integrins, in the recognition of the V2 module. This conclusion was also consistent with the observed differential behavior of wild-type CHO cells which, in both systems, were less sensitive to V2 concentration than  $\beta_3$ -CHO and  $\alpha_{IIb}\beta_3$ -CHO cells (Fig. 5, *A* and *B*). Similar experiments were performed using EGF-RGD, yielding comparable inhibition patterns, although with much lower inhibitory effects, reaching maximal values of 13% in the case of fibronectin and 21% in the case of fibrinogen (data not shown).

**Surface Plasmon Resonance Analysis of the Interaction between Purified Integrins and the Chimeric EGF Modules**—

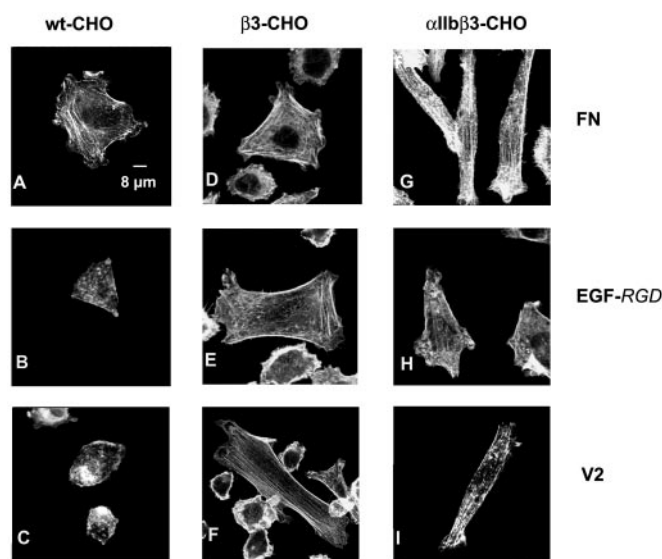


FIG. 4. Visualization of stress fibers in different CHO cell lines bound to fibronectin, the EGF-RGD, and V2 modules. Wild-type (*wt*) CHO cells (A–C),  $\beta_3$ -CHO cells (D–F), and  $\alpha_{11b}\beta_3$ -CHO cells (G–I) were allowed to attach for 2 h at 37 °C on glass slides coated with fibronectin (FN; A, D, and G), EGF-RGD (B, E, and H), or the V2 variant (C, F, and I). Actin stress fibers were decorated with rhodamine-conjugated phalloidin. The bar represents 8  $\mu$ m.

Detailed information on the binding properties of the EGF-RGD and V2 modules was obtained by surface plasmon resonance spectroscopy, using the modules as immobilized ligands and purified  $\alpha_v\beta_3$  and  $\alpha_5\beta_1$  integrins as soluble analytes, as described under “Experimental Procedures.” Initial experiments showed that the integrins did not bind to an unrelated protein (bovine serum albumin) or to the native C1r EGF module. As illustrated in Fig. 6,  $\alpha_5\beta_1$  and  $\alpha_v\beta_3$  both readily bound to the immobilized EGF-RGD and V2 modules in the presence of  $MgCl_2$  and  $CaCl_2$ . No binding was observed in the presence of 1 mM EDTA (data not shown). Each integrin showed comparable association and dissociation curves on both modules, with a much faster dissociation phase for  $\alpha_5\beta_1$  (Fig. 6, A and B) than for  $\alpha_v\beta_3$  (Fig. 6, C and D). The kinetic parameters of the interactions were determined by recording sensograms at different integrin concentrations. The association ( $k_{on}$ ) and dissociation ( $k_{off}$ ) rate constants, and the resulting apparent equilibrium constant  $K_D$  are shown in Table II.  $\alpha_5\beta_1$  exhibited higher  $k_{on}$  values for both modules whereas, conversely,  $\alpha_v\beta_3$  showed lower  $k_{off}$  values. For both integrins, V2 was found to be a better ligand than EGF-RGD, because of decreased  $k_{off}$  values and, in the case of  $\alpha_5\beta_1$ , to an increased  $k_{on}$  value. The resulting  $K_D$  range from 31.5 nM for the interaction between  $\alpha_5\beta_1$  and EGF-RGD to 3.5 nM for the interaction between  $\alpha_v\beta_3$  and V2. As discussed below, these values are comparable with those determined for the binding of these integrins to their natural ligands.

$\alpha_v$  Integrin from a CHO Cell Lysate Binds to a Nickel-Sephacrose-Trx-V2 Column—We next tested whether integrins from a total  $\alpha_{11b}\beta_3$ -CHO cell lysate, containing  $\alpha_v$ ,  $\alpha_{11b}$ , and  $\alpha_5$  integrins, were able to interact with the Trx-V2 fusion protein non-covalently coupled on a nickel-Sephacrose resin. The fusion protein was first incubated with the nickel-Sephacrose resin and then the resin was suspended in a crude  $\alpha_{11b}\beta_3$ -CHO cell lysate for 2.5 h at room temperature. After extensive washes, bound proteins were eluted with EDTA and analyzed by SDS-PAGE and Western blotting using polyclonal anti- $\alpha_v$  antibodies. As shown in Fig. 7,  $\alpha_v$  was specifically detected in the sample eluted from the Trx-V2 resin (Fig. 7, lane 9) but not from a control sample eluted from a Trx-C1r EGF resin (Fig. 7, lane 8).

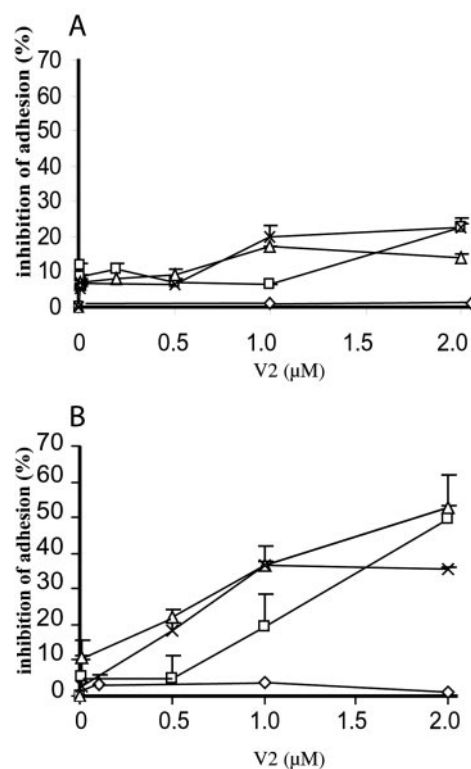


FIG. 5. Inhibition by the V2 module of cell adhesion to matrix proteins. Cells were preincubated with the soluble V2 module at the indicated concentrations for 15 min at 4 °C and then allowed to attach, in the absence of serum, to fibronectin (A) or fibrinogen (B). Cell adhesion was quantified using the colorimetric assay described under “Experimental Procedures.” Results are expressed relative to the maximal adhesion value measured in the absence of competitor. Each data point represents the mean  $\pm$  S.D. from three independent experiments. □, wild-type CHO cells; Δ,  $\beta_3$ -CHO cells; X,  $\alpha_{11b}\beta_3$ -CHO cells; ◇, control experiments obtained with  $\beta_3$ -CHO cells incubated with the unmodified C1r EGF module. Similar control curves were obtained for wild-type CHO cells and  $\alpha_{11b}\beta_3$ -CHO cells.

The nickel-Sephacrose resin alone showed no binding (Fig. 7, lane 7). Similar experiments designed to detect specifically the  $\alpha_5$  or  $\alpha_{11b}$  integrins were both unsuccessful (data not shown). These data provided direct evidence of the ability of the  $\alpha_v\beta_3$  integrin expressed by the  $\alpha_{11b}\beta_3$ -CHO cells to associate with the V2 module in such a way that allows formation of a stable complex on the nickel-Sephacrose resin. Such a stability is likely rendered possible by the low dissociation rate constant of the interaction, as observed by surface plasmon resonance analysis (Fig. 6).

**Comparative Analysis by NMR of the EGF-RGD and V2 Modules**—NMR spectroscopy was used to obtain detailed structural and dynamic information on the two modules. Assignment of the  $^1H$  and  $^{15}N$  frequencies of the backbone amides was performed using two-dimensional TOCSY and NOESY, as well as a three-dimensional NOESY-HSQC experiments. For both modules, assignment could be obtained for all residues except Gly<sup>28</sup> and a stretch from Pro<sup>15</sup> to Cys<sup>19</sup>. Comparison of the  $^1H$  frequencies of EGF-RGD and V2 with those of the native C1r EGF module (27) revealed significant similarity in the C-terminal part and indicated that the loop between the first two cysteines was also disordered in the RGD-containing modules. Further structural analysis of the EGF-RGD and V2 modules based on a detailed comparison of their NOE patterns in the three-dimensional NOESY-HSQC experiments showed no significant variation in peak intensity or cross-peak pattern. It was concluded therefore that the overall EGF module fold was maintained in both modules, the loop harboring the RGD se-

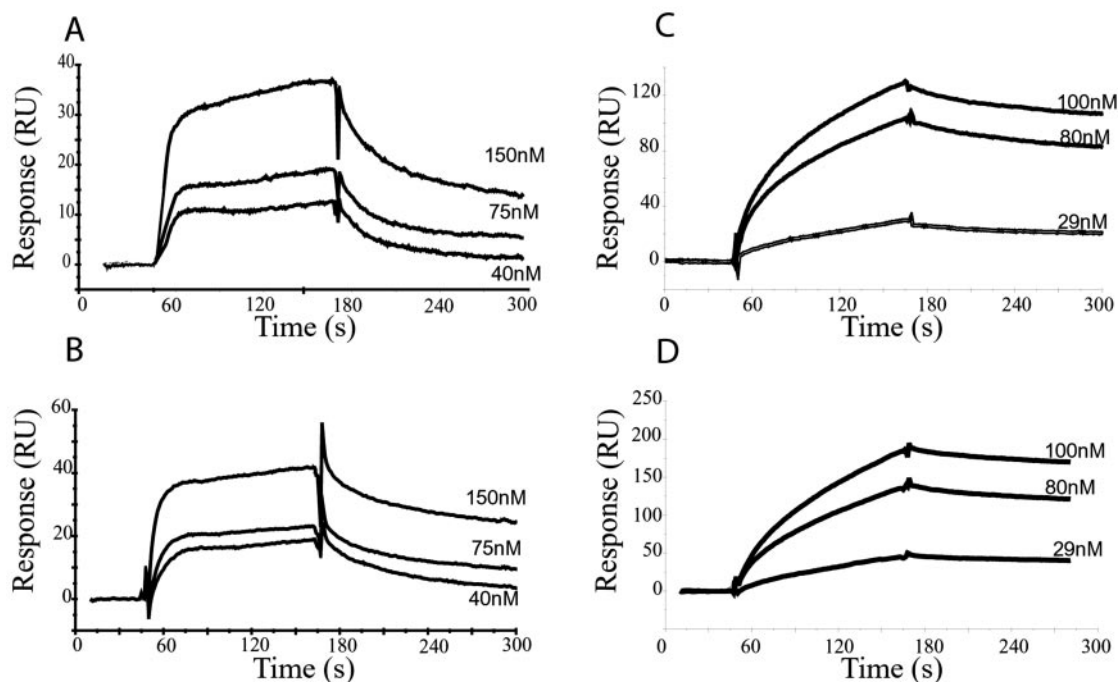


FIG. 6. Surface plasmon resonance analysis of the binding of  $\alpha_v\beta_3$  and  $\alpha_5\beta_1$  to the EGF-RGD and V2 modules. The chimeric modules were immobilized onto the carboxymethylated dextran surface of a CM5 sensorchip using the amine coupling chemistry. Binding of the purified integrins was measured simultaneously to immobilized EGF-RGD or V2 or to an activated-deactivated surface in the running buffer (150 mM NaCl, 25 mM Tris-HCl, pH 7.4, 0.1 mM  $\text{CaCl}_2$ , 1 mM  $\text{MgCl}_2$ , 10 mM octyl- $\beta$ -D-glucopyranoside) at a flow rate of 20  $\mu\text{l}/\text{min}$  using a BIACORE 3000 apparatus. Association and dissociation curves are shown for different  $\alpha_v\beta_3$  or  $\alpha_5\beta_1$  integrin concentrations. The specific binding signal shown was obtained by subtracting the background signal (obtained by injection of the protein sample over a activated-deactivated surface). A, interaction between  $\alpha_5\beta_1$  and EGF-RGD. B, interaction between  $\alpha_5\beta_1$  and V2. C, interaction between  $\alpha_v\beta_3$  and EGF-RGD. D, interaction between  $\alpha_v\beta_3$  and V2.

TABLE II

Kinetic and dissociation constants for the interaction of  $\alpha_5\beta_1$  and  $\alpha_v\beta_3$  with the immobilized EGF-RGD and V2 modules

The association ( $k_{\text{on}}$ ) and dissociation ( $k_{\text{off}}$ ) rate constants were determined by global fitting of the data using a 1:1 Langmuir binding model (BIAevaluation 3). The dissociation constants  $K_D$  were determined from the  $k_{\text{off}}/k_{\text{on}}$  ratio.

| Ligand  | $\alpha_5\beta_1$                  |                              |               | $\alpha_v\beta_3$                  |                              |               |
|---------|------------------------------------|------------------------------|---------------|------------------------------------|------------------------------|---------------|
|         | $k_{\text{on}}$<br>$M^{-1} s^{-1}$ | $k_{\text{off}}$<br>$s^{-1}$ | $K_D$<br>$nM$ | $K_{\text{on}}$<br>$M^{-1} s^{-1}$ | $K_{\text{off}}$<br>$s^{-1}$ | $K_D$<br>$nM$ |
| EGF-RGD | $0.8 \times 10^6$                  | $2.56 \times 10^{-2}$        | 31.5          | $2.2 \times 10^5$                  | $1.1 \times 10^{-3}$         | 5.1           |
| V2      | $1.5 \times 10^6$                  | $1.09 \times 10^{-2}$        | 7.2           | $1.7 \times 10^5$                  | $0.6 \times 10^{-3}$         | 3.5           |

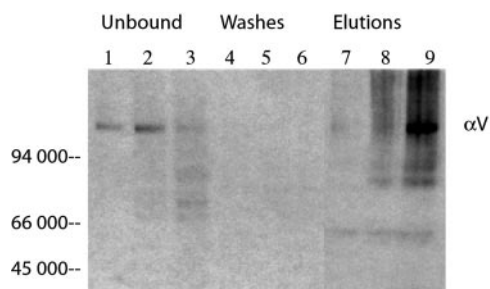


FIG. 7. The  $\alpha_v$  integrin subunit from a  $\alpha_{III}\beta_3$ -CHO cell lysate binds to a nickel-Sepharose-Trx-V2 resin. Samples eluted from a free nickel-Sepharose resin (lanes 1, 4, and 7), a nickel-Sepharose-Trx-C1r EGF resin (lanes 2, 5, and 8), or a nickel-Sepharose-Trx-V2 resin (lanes 3, 6, and 9) were separated on a 7.5% polyacrylamide SDS-PAGE under non-reducing conditions and then analyzed by Western blotting using polyclonal antibodies directed against the  $\alpha_v$  integrin subunit. Unbound fractions (lanes 1–3), washes (lanes 4–6), and EDTA/NaCl elution fractions (lanes 7–9) are shown for the three resin types. Positions of molecular mass markers are shown. The  $\alpha_v$  integrin subunit (apparent molecular mass 150,000 Da) is detected in the unbound material from the free nickel-Sepharose (lane 1) and nickel-Sepharose-Trx-C1r EGF resins (lane 2), as well as in the fraction eluted from the nickel-Sepharose-Trx-V2 resin (lane 9).

quence being flexible in both cases.

NMR spectroscopy also offers the possibility to characterize protein dynamics at the residue level by measuring different

$^{15}\text{N}$  relaxation rates ( $R_1$ ,  $R_2$ ) and the  $\{^1\text{H}\}$ - $^{15}\text{N}$  NOE, which are dependent on the mobility of the  $^{15}\text{N}$ - $^1\text{H}$  vectors in the pico- to nanosecond time scale. In addition, the  $R_2$  relaxation rate can also include a contribution from a local chemical or conformational exchange. Relaxation rates could be determined for 38 of the 43 assigned residues in the case of EGF-RGD and for 34 of the 41 assigned residues for V2. This confirmed that both modules comprise a relatively flexible N-terminal part, characterized by low  $\{^1\text{H}\}$ - $^{15}\text{N}$  NOE values (Fig. 8A) and low  $R_1$  and/or  $R_2$  relaxation rates (Fig. 8B) and a more rigid C-terminal part, in keeping with our previous analysis of the native C1r EGF module (27). Detailed comparative analysis of these data for the two modules revealed very similar values for the  $R_1$  rate constants and the  $\{^1\text{H}\}$ - $^{15}\text{N}$  NOE values, which both sample internal motion at the pico- to nanosecond time scale. In contrast, significant differences in the  $R_2$  rate constants can be observed, notably at the level of the RGD motif (Fig. 8B), which shows significantly higher values in V2 than in EGF-RGD. It was not possible to precisely measure the overall rotational correlation time of each module, a prerequisite for a detailed motional analysis based on the model-free approach proposed by Lipari and Szabo (44). Thus, although our data clearly suggest that the different affinities of the modules for integrins are related to a differential motional behavior, it cannot be concluded whether this difference arises from a slow

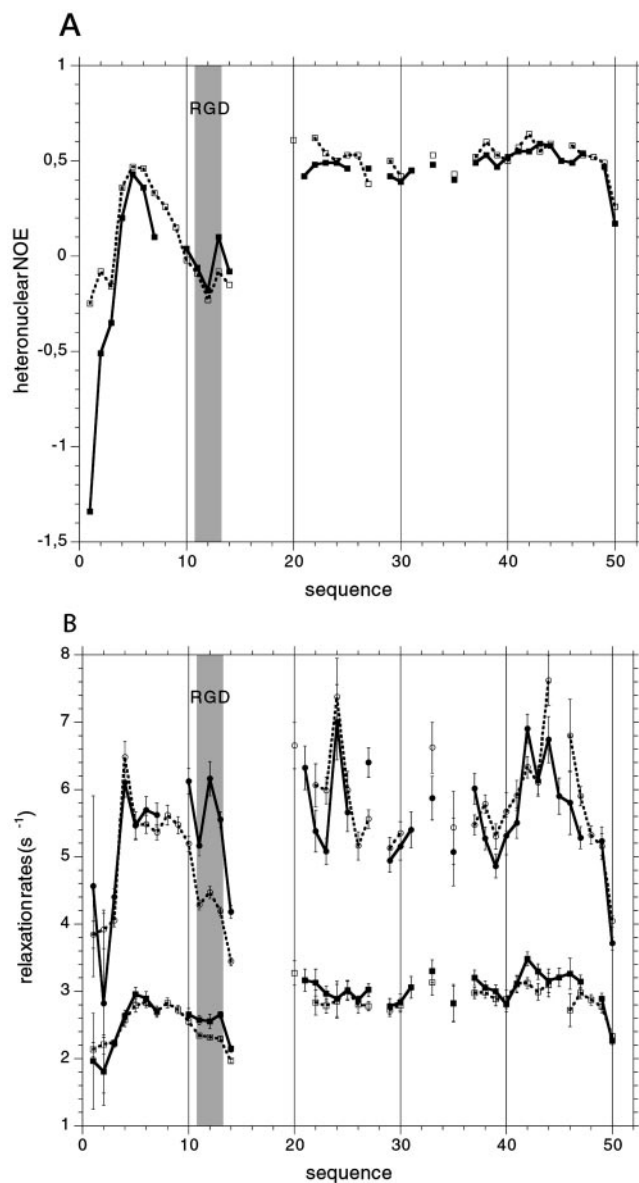


FIG. 8. Comparative  $^{15}\text{N}$  relaxation data for EGF-RGD and V2. Heteronuclear NOE values (A) and  $^{15}\text{N}$  relaxation rates (B) of  $R_1$  (squares) and  $R_2$  (circles) as a function of protein sequence are shown. Open symbols and dotted line, EGF-RGD module; filled symbols and continuous line, V2 module. Error bars in B indicate the uncertainties estimated from a Monte-Carlo analysis. The location of the RGD sequence is indicated. Note that residues 8 and 9 are not present in the V2 sequence, the numbering being otherwise identical for both modules for the sake of clarity (see Fig. 1).

conformational reorientation of the RGD motif in V2 or a higher mobility in EGF-RGD.

#### DISCUSSION

The present study describes an efficient method for the production in a bacterial expression system of engineered EGF-like modules containing an RGD sequence and their use as high affinity ligands for cell surface integrins. The system used is based on expression of Trx fusion proteins and allows production of recombinant EGF-like modules in a soluble form, at a high yield and with a conformation that retains the natural folding of the human C1r EGF module used as a protein scaffold, namely the Cys<sup>1</sup>-Cys<sup>3</sup>, Cys<sup>2</sup>-Cys<sup>4</sup>, Cys<sup>5</sup>-Cys<sup>6</sup> disulfide bridge pattern characteristic of EGF-like modules. Based on the analogy with the RGD-containing domain of snake disintegrins, our original EGF-RGD module was modified by decreasing the length of the

RGD-containing loop and thereby changing the position of the RGD motif within the loop, leading to the V2 variant.

The EGF-RGD and V2 modules have been characterized functionally using various methods aimed at measuring their ability to promote cell adhesion, to inhibit cell adhesion to natural ligands, to induce signal transduction, and to associate with particular integrins using a resin binding assay and direct analysis by surface plasmon resonance spectroscopy. Based on these different assays, it may be concluded that the EGF-RGD and V2 modules both exhibit preferential binding to  $\beta_3$  integrins, compared with  $\beta_1$  integrins. This conclusion is based on the following observations. (i) When coated on a surface both modules yielded high adhesion levels in the case of  $\beta_3$ -CHO cells (expressing  $\alpha_v\beta_3$ ) and  $\alpha_{\text{IIb}}\beta_3$ -CHO cells (predominantly expressing  $\alpha_{\text{IIb}}\beta_3$ ). In contrast, significantly lower adhesion levels were observed in the case of wild-type CHO cells (only expressing  $\beta_1$  integrins), and adhesion in this case was strictly dependent on the presence of serum, suggesting the requirement of one or more additional factors from serum, possibly endogenous plasmatic ligands or growth factors. (ii) As revealed by visualization of actin stress fibers, cell adhesion led to intracellular signaling for both  $\beta_3$ -CHO and  $\alpha_{\text{IIb}}\beta_3$ -CHO cells but not for wild-type CHO cells. (iii) In competition assays, the soluble V2 module strongly inhibited cell adhesion to fibrinogen (the major ligand of  $\alpha_v\beta_3$  and  $\alpha_{\text{IIb}}\beta_3$ ) and only poorly inhibited cell adhesion to fibronectin (the major ligand of  $\alpha_5\beta_1$ ). In addition, for both ligands, wild-type CHO cells were significantly less sensitive to V2 concentration than  $\beta_3$ -transfected cells (see Fig. 5). (iv) As shown by direct surface plasmon resonance analysis using purified integrins, the EGF-RGD and V2 modules exhibit significantly higher affinities for  $\alpha_v\beta_3$  than for  $\alpha_5\beta_1$ , essentially because of a lower dissociation rate constant. In this respect, however, it should be emphasized that the affinity of the V2 variant for purified  $\alpha_5\beta_1$  ( $K_D = 7.2$  nM) is not strikingly lower than that for  $\alpha_v\beta_3$  ( $K_D = 3.5$  nM). Despite this similarity, V2 efficiently triggers intracellular signaling in  $\beta_3$ -transfected cell lines and has no detectable effect on wild-type CHO cells (see Fig. 4), consistent with the fact that, unlike  $\beta_3$  integrins, signaling by  $\beta_1$  integrins not only involves binding to an RGD motif but also requires recognition of a synergy sequence, such as the Pro-His-Ser-Arg-Asn motif present on fibronectin (45).

Another conclusion that can be drawn from our data is that the modification converting EGF-RGD into V2 has more impact on  $\alpha_5\beta_1$  than on  $\beta_3$  integrins. Thus, analysis by surface plasmon resonance spectroscopy clearly indicates that this modification results in a 4-fold decrease in  $K_D$  for  $\alpha_5\beta_1$ , compared with only 1.5 in the case of  $\alpha_v\beta_3$ . This 4-fold  $K_D$  decrease is indeed very close to the increase in adhesion observed for wild-type CHO cells (Fig. 3B), providing strong support for the hypothesis that, in the case of  $\beta_3$ -transfected cells as well, the observed increased adhesion on V2 may be due, for a large part, to the better affinity of this module for  $\alpha_5\beta_1$  integrins.

Other observations appear consistent with the hypothesis that, in their soluble form, the recombinant modules recognize  $\alpha_v\beta_3$  preferentially to  $\alpha_{\text{IIb}}\beta_3$ . Thus, binding assays using the Trx-V2 construct attached to a nickel-Sepharose resin resulted in the specific capture of the  $\alpha_v$  subunit from a  $\alpha_{\text{IIb}}\beta_3$ -CHO cell lysate and showed no evidence for binding of the  $\alpha_{\text{IIb}}$  or  $\alpha_5$  subunits. This is in agreement with the fact that  $\alpha_{\text{IIb}}\beta_3$ -CHO cells express the  $\alpha_{\text{IIb}}\beta_3$  integrin in a resting state with only low affinity for soluble ligands, including fibrinogen (46, 47). Further support for this hypothesis arises from the observation that, in competition experiments, compared with  $\beta_3$ -CHO cells, adhesion of  $\alpha_{\text{IIb}}\beta_3$ -CHO cells to fibrinogen was slightly but consistently less sensitive to inhibition by the soluble V2 mod-

ule (see Fig. 5B), again suggesting a better affinity of this module for  $\alpha_v\beta_3$  in this cellular model. Further experiments, such as surface plasmon resonance analysis of the interaction between the chimeric EGF modules and a purified  $\alpha_{\text{IIb}}\beta_3$  fraction, will be necessary to reach a more definitive conclusion on this question.

Direct analysis of the interaction between the immobilized EGF-RGD and V2 modules and the purified  $\alpha_v\beta_3$  and  $\alpha_5\beta_1$  integrins used as soluble analytes yielded  $K_D$  values ranging from 3.5 to 31.5 nM. These values are comparable with those determined by the same method for the interaction of integrins with their natural ligands such as between  $\alpha_v\beta_3$  and osteopontin ( $K_D = 0.43$  nM) (48),  $\alpha_v\beta_3$  and the P1 fragment of laminin ( $K_D = 450$  nM) (49), or  $\alpha_{\text{IIb}}\beta_3$  and fibrinogen ( $K_D = 20$ –70 nM) (50). For comparison, the affinity determined for the binding of the Fab-9 antibody to the  $\alpha_{\text{IIb}}\beta_3$  integrin was also in the nanomolar range (51). Likewise, although no data based on surface plasmon resonance analysis are currently available for the interaction between integrins and disintegrins, the affinities estimated by Scatchard analysis are in the nanomolar range (52). In contrast, integrins were found to bind to cyclic RGD peptides with affinities in the micromolar range or higher (53). The disintegrin-like V2 module exhibited enhanced binding affinities compared with the original EGF-RGD module, especially in the case of  $\alpha_5\beta_1$ . Remarkably, the modifications leading to the V2 variant had differential effects on the interaction with  $\alpha_v\beta_3$  and  $\alpha_5\beta_1$ , with a decreased  $k_{\text{off}}$  value in both cases and an increased  $k_{\text{on}}$  value in the latter case only. This observation implies that it should be feasible, by introducing further modifications within the RGD-containing loop of the EGF module, to design variants with improved affinity for a particular integrin and decreased affinities for others.

In this respect, NMR analysis of the EGF-RGD and V2 variants provided clear evidence that, in both cases, modifications in the RGD-containing loop had no impact on the C-terminal part of the EGF module, which, as judged from all measurements, retained a structured  $\beta$ -sheet fold comparable with that described for the unmodified C1r EGF module (27). This observation opens the way to a large variety of changes within the loop, in terms of both length and amino acid content. Interestingly, NMR analysis revealed a differential dynamic behavior of the RGD motif in the EGF-RGD and V2 modules, suggesting that their different reactivity with integrins arises either from a slow conformational reorientation of the RGD motif in V2 or a higher mobility in EGF-RGD. Interestingly, NMR relaxation studies performed on the tenth type III domain of fibronectin indicate that the RGD sequence is subject to very rapid local motions (54–56). In contrast, in the third type III domain of tenascin-C, the RGD motif is presented on a rigid tight turn (55). Taken together, these data suggest that the intrinsic mobility of the RGD motif within an integrin ligand may affect either positively or negatively its reactivity, depending on the target integrin.

Altogether, the results presented in this study establish that chimeric RGD-containing EGF modules interact with high affinity with integrins and show a functional preference for  $\alpha_v\beta_3$ , which is involved in numerous pathological processes such as tumor vascularization, cancer metastasis, or bone resorption. As detailed above, it seems quite feasible to design improved variants with selective binding properties for particular integrins. In addition, the observation that the integrin binding ability of these modules is retained in Trx fusion proteins validates the possibility of incorporating them into multimodular proteins to use them as carriers for other biologically active modules. We believe that these chimeric modules represent valuable tools for cell targeting, without the limitations en-

countered with other carrier systems such as peptides, phages, and viruses (16, 25, 57, 58).

**Acknowledgments**—We are grateful to Alain Duperray for the gift of the  $\beta_3$ -CHO and  $\alpha_{\text{IIb}}\beta_3$ -CHO cell lines. We thank Jean-Pierre Andrieu for determining N-terminal sequences, Didier Grunwald for confocal microscopy, and David Lascoux and Bernard Dublet for performing mass spectrometry analyses.

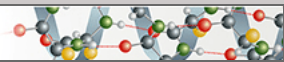
## REFERENCES

- Hynes, R. O. (1992) *Cell* **69**, 11–25
- Hynes, R. O. (1996) *Dev. Biol.* **180**, 402–412
- Hynes, R. O., and Wagner, D. D. (1996) *J. Clin. Invest.* **98**, 2193–2195
- Schwartz, M. A., Schaller, M. D., and Ginsberg, M. H. (1995) *Annu. Rev. Cell Dev. Biol.* **11**, 549–599
- Plow, E. F., Haas, T. A., Zhang, L., Loftus, J., and Smith, J. W. (2000) *J. Biol. Chem.* **275**, 21785–21788
- Danen, E. H., and Yamada, K. M. (2001) *J. Cell. Physiol.* **189**, 1–13
- Yamada, K. M., and Even-Ram, S. (2002) *Nat. Cell Biol.* **4**, E75–76
- Eliceiri, B. P., and Cheresch, D. A. (1998) *Mol. Med.* **4**, 741–750
- Eliceiri, B. P., and Cheresch, D. A. (1999) *J. Clin. Invest.* **103**, 1227–1230
- Mizejewski, G. J. (1999) *Proc. Soc. Exp. Biol. Med.* **222**, 124–138
- Varner, J. A., and Cheresch, D. A. (1996) *Curr. Opin. Cell Biol.* **8**, 724–730
- Ruoslahti, E. (1999) *Adv. Cancer Res.* **76**, 1–20
- Felding-Habermann, B., O'Toole, T. E., Smith, J. W., Fransvea, E., Ruggeri, Z. M., Ginsberg, M. H., Hughes, P. E., Pampori, N., Shattil, S. J., Saven, A., and Mueller, B. M. (2001) *Proc. Natl. Acad. Sci. U. S. A.* **98**, 1853–1858
- Watt, F. M. (2002) *EMBO J.* **21**, 3919–3926
- Pecheur, I., Peyruchaud, O., Serre, C. M., Guglielmi, J., Voland, C., Bourre, F., Margue, C., Cohen-Solal, M., Buffet, A., Kieffer, N., and Clezardin, P. (2002) *FASEB J.* **16**, 1266–1268
- Colin, M., Maurice, M., Trugnan, G., Kornprobst, M., Harbottle, R. P., Knight, A., Cooper, R. G., Miller, A. D., Capeau, J., Coutelle, C., and Brahimi-Horn, M. C. (2000) *Gene Ther.* **7**, 139–152
- Ruoslahti, E., and Pierschbacher, M. D. (1986) *Cell* **44**, 517–518
- Xiong, J. P., Stehle, T., Diefenbach, B., Zhang, R., Dunker, R., Scott, D. L., Joachimiak, A., Goodman, S. L., and Arnaut, M. A. (2001) *Science* **294**, 339–345
- Xiong, J. P., Stehle, T., Zhang, R., Joachimiak, A., Frech, M., Goodman, S. L., and Arnaut, M. A. (2002) *Science* **296**, 151–155
- Gould, R. J., Polokoff, M. A., Friedman, P. A., Huang, T. F., Holt, J. C., Cook, J. J., and Niewiarowski, S. (1990) *Proc. Soc. Exp. Biol. Med.* **195**, 168–171
- Weskamp, G., and Blobel, C. P. (1994) *Proc. Natl. Acad. Sci. U. S. A.* **91**, 2748–2751
- Primakoff, P., and Myles, D. G. (2000) *Trends Genet.* **16**, 83–87
- Saudek, V., Atkinson, R. A., Lepage, P., and Pelton, J. T. (1991) *Eur. J. Biochem.* **202**, 329–338
- Blobel, C. P., and White, J. M. (1992) *Curr. Opin. Cell Biol.* **4**, 760–765
- Parkes, R. J., and Hart, S. L. (2000) *Adv. Drug. Deliv. Rev.* **44**, 135–152
- Hernandez, J. F., Bersch, B., Petillot, Y., Gagnon, J., and Arlaud, G. J. (1997) *J. Pept. Res.* **49**, 221–231
- Bersch, B., Hernandez, J. F., Marion, D., and Arlaud, G. J. (1998) *Biochemistry* **37**, 1204–1214
- Campbell, I. D., and Bork, P. (1993) *Curr. Opin. Struct. Biol.* **3**, 385–392
- Bork, P., Downing, A. K., Kieffer, B., and Campbell, I. D. (1996) *Q. Rev. Biophys.* **29**, 119–167
- Vella, F., Hernandez, J. F., Molla, A., Block, M. R., and Arlaud, G. J. (1999) *J. Pept. Res.* **54**, 415–426
- Frachet, P., Uzan, G., Thevenon, D., Denarier, E., Prandini, M. H., and Marguerie, G. (1990) *Mol. Biol. Rep.* **14**, 27–33
- Arlaud, G. J., Reboul, A., Meyer, C. M., and Colomb, M. G. (1977) *Biochim. Biophys. Acta* **485**, 215–225
- Journet, A., and Tosi, M. (1986) *Biochem. J.* **240**, 783–787
- Ho, S. N., Hunt, H. D., Horton, R. M., Pullen, J. K., and Pease, L. R. (1989) *Gene* **77**, 51–59
- Horton, R. M., Cai, Z. L., Ho, S. N., and Pease, L. R. (1990) *BioTechniques* **8**, 528–535
- Jansson, M., Li, Y. C., Jendeborg, L., Anderson, S., Montelione, B. T., and Nilsson, B. (1996) *J. Biomol. NMR* **7**, 131–141
- Laemmli, U. K. (1970) *Nature* **227**, 680–685
- Rossi, V., Bally, I., Thielens, N. M., Esser, A. F., and Arlaud, G. J. (1998) *J. Biol. Chem.* **273**, 1232–1239
- Markley, J. L., Bax, A., Arata, Y., Hilbers, C. W., Kaptein, R., Sykes, B. D., Wright, P. E., and Wuthrich, K. (1998) *J. Mol. Biol.* **280**, 933–952
- Farrow, N. A., Muhandiram, R., Singer, A. U., Pascal, S. M., Kay, C. M., Gish, G., Shoelson, S. E., Pawson, T., Forman-Kay, J. D., and Kay, L. E. (1994) *Biochemistry* **33**, 5984–6003
- Defilippi, P., Venturino, M., Gulino, D., Duperray, A., Boquet, P., Fiorentini, C., Volpe, G., Palmieri, M., Silengo, L., and Tarone, G. (1997) *J. Biol. Chem.* **272**, 21726–21734
- Frachet, P., Duperray, A., Delachanal, E., and Marguerie, G. (1992) *Biochemistry* **31**, 2408–2415
- Hantgan, R. R., Endenburg, S. C., Cavero, I., Marguerie, G., Uzan, A., Sixma, J. J., and de Groot, P. G. (1992) *Thromb. Haemost.* **68**, 694–700
- Lipari, G., and Szabo, A. (1982) *J. Am. Chem. Soc.*, 4546–4558
- Aota, S., Nomizu, M., and Yamada, K. M. (1994) *J. Biol. Chem.* **269**, 24756–24761
- Kamata, T., Irie, A., Tokuhira, M., and Takada, Y. (1996) *J. Biol. Chem.* **271**, 18610–18615
- O'Toole, T. E., Loftus, J. C., Du, X. P., Glass, A. A., Ruggeri, Z. M., Shattil, S. J., Plow, E. F., and Ginsberg, M. H. (1990) *Cell Regul.* **1**, 883–893

48. Hu, D. D., Hoyer, J. R., and Smith, J. W. (1995) *J. Biol. Chem.* **270**, 9917–9925
49. Pfaff, M., Gohring, W., Brown, J. C., and Timpl, R. (1994) *Eur. J. Biochem.* **225**, 975–984
50. Huber, W., Hurst, J., Schlatter, D., Barner, R., Hubscher, J., Kouns, W. C., and Steiner, B. (1995) *Eur. J. Biochem.* **227**, 647–656
51. Hu, D. D., Barbas, C. F., and Smith, J. W. (1996) *J. Biol. Chem.* **271**, 21745–21751
52. Marcinkiewicz, C., Vijay-Kumar, S., McLane, M. A., and Niewiarowski, S. (1997) *Blood* **90**, 1565–1575
53. Hu, B., Finsinger, D., Peter, K., Guttenberg, Z., Barmann, M., Kessler, H., Escherich, A., Moroder, L., Bohm, J., Baumeister, W., Sui, S. F., and Sackmann, E. (2000) *Biochemistry* **39**, 12284–12294
54. Spitzfaden, C., Grant, R. P., Mardon, H. J., and Campbell, I. D. (1997) *J. Mol. Biol.* **265**, 565–579
55. Carr, P. A., Erickson, H. P., and Palmer, A. G., III (1997) *Structure* **5**, 949–959
56. Copie, V., Tomita, Y., Akiyama, S. K., Aota, S., Yamada, K. M., Venable, R. M., Pastor, R. W., Krueger, S., and Torchia, D. A. (1998) *J. Mol. Biol.* **277**, 663–682
57. Jenkins, R. G., Herrick, S. E., Meng, Q. H., Kinnon, C., Laurent, G. J., McAnulty, R. J., and Hart, S. L. (2000) *Gene Ther.* **7**, 393–400
58. O'Neal, W. K., Zhou, H., Morral, N., Langston, C., Parks, R. J., Graham, F. L., Kochanek, S., and Beaudet, A. L. (2000) *Mol. Med.* **6**, 179–195

**Protein Structure and Folding:  
A Recombinant Chimeric Epidermal  
Growth Factor-like Module with High  
Binding Affinity for Integrins**

PROTEIN STRUCTURE  
AND FOLDING



Fanny Vella, Nicole M. Thielens, Beate  
Bersch, Gérard J. Arlaud and Philippe Frchet  
*J. Biol. Chem.* 2003, 278:19834-19843.

doi: 10.1074/jbc.M301470200 originally published online March 24, 2003

---

Access the most updated version of this article at doi: [10.1074/jbc.M301470200](https://doi.org/10.1074/jbc.M301470200)

Find articles, minireviews, Reflections and Classics on similar topics on the [JBC Affinity Sites](#).

Alerts:

- [When this article is cited](#)
- [When a correction for this article is posted](#)

[Click here](#) to choose from all of JBC's e-mail alerts

This article cites 57 references, 17 of which can be accessed free at  
<http://www.jbc.org/content/278/22/19834.full.html#ref-list-1>